Damage and failure prediction in Alumina Tri-Hydrate/Epoxy core composite sandwich panels subjected to impact loads

G. Morada[1], R. Ouadday[1], †A. Marouene[1], *A. Vadean[1], and R. Boukhili[1]

[1]Department of Mechanical engineering, Polytechnique Montreal, Montreal, Quebec, Canada.

*Presenting author: aurelian.vadean@polymtl.ca

†Corresponding author: aymen.marouene@polymtl.ca

Abstract

This paper reports an experimental and numerical analysis of the impact behavior of composite sandwich panels. An innovative sandwich construction with an ATH/Epoxy core (i.e. epoxy resin filled with alumina tri-hydrate (ATH) particles) and non-crimp glass fabric fibre-reinforced epoxy face-sheets was subjected to impact loads. Explicit nonlinear finite elements model was developed to predict the damage characteristics in both the face-sheets and core. The obtained numerical results were compared with the test data to assess the effectiveness of the proposed model. A good correlation with respect to the contact force and energy-time relationships, permanent deformation, and impact-induced damage was achieved. The contribution of each component of the sandwich structure to its energy absorption capabilities was also evaluated. It was found, for an impact energy of 21J, that the energy dissipated in the ATH/Epoxy core is almost two times more than that dissipated in the face-sheets. The important role of the core material for reducing face-sheet damage was identified.

Keywords: Impact behaviour, Composite sandwich panel, Alumina trihydrate (ATH) particles, damage mechanisms.

Introduction

Composite sandwich structures are finding increasing utilization in many engineering applications such as the aerospace, automotive, building, and water turbine industries, because of their relative benefits over other structural materials [1]. For instance, conventional structures in hydraulic turbine are nowadays replaced with composite sandwich structures to improve energy production and to facilitate in-site manufacturing. However, in such application, it has been found that the river flow can provoke huge amount of waterborne debris and the waterborne debris impact was highlighted as a major source of damage for the composite hydraulic turbine blades. Therefore, impact resistance is an important topic in engineering communities.

Impact resistance of composite sandwich depend on the mechanical and geometrical properties of its constituents such as the face-sheet material, core material, and the adhesive interface properties. Core crushing was identified as the major failure mechanism under an impact event [2]. Meanwhile, one major drawback of sandwich structures is its poor transverse stiffness [3]. Therefore, the core material properties are the main parameters to improve impact resistance of composite sandwich panels. A wide variety of material can be used as core in sandwich constructions such as synthetic foam, honeycomb, balsa wood, and corrugated cores among others [1]. The main functions of the core materials are to absorb impact energies and provide the overall bending resistance. However, the problem with light-weight cores is that they are not enough resistant to withstand high impact loads.

Mines et al. [2] reported that the core density affects the failure progression. Furthermore, it has been shown that absorbing impact energy via the plastic deformations of the core can improve the damage tolerance of sandwich structures [4]. Torre and Kenny [5] used an innovative sandwich construction made of glass/phenolic composite skins and a rigid polymer foam core with fibre reinforced plastic to enhance crush resistance for civil engineering structures. The sandwich addressed herein is a high density core made of epoxy resin filled with Alumina tri-hydrate particles. This sandwich construction was designed to increase the core crushing resistance and hence improve damage tolerance of sandwich panels at high impact loads.

In light of the aforementioned considerations and the existence of some limitations for performing experimental tests, there is a strong need to develop a numerical model that can be used to predict the structural impact response and the damage process and locations under impact conditions.

There are several numerical approaches reported in the open literature for prediction of the response of sandwich structures under impact loads. In order to reduce the computational time, some researchers [6-8] have used 2D shell elements to model the face-sheets. Among them, Zhou et al. [6] studied the perforation resistance of foam-based sandwich panels using 2D elements for the face-sheets, however, it should be noted that these elements are not accurate for failure analysis since the stress distribution in the face-sheets is a 3D problem. Feng et al. [9] used a progressive damage model to simulate the damage scenarios in foam-based sandwich composites subjected to impact loads. In their proposed model, a 3D damage model was used to track the intra-laminar damages in face-sheets and cohesive elements were used to simulate interface delaminations.

The objective of this work is to investigate the impact response of a particular composite sandwich panel designed to the water turbine industries. This sandwich is made of a high-density core (ATH/Epoxy: epoxy resin filled with alumina trihydrate particles) and Non-Crimp Fabrics glass/epoxy skins. To the best of the authors’ knowledge, there is no published studies deal with this sandwich construction. A numerical 3D continuum model was implemented in LS-DYNA/Explicit code to simulate the intra-laminar damage initiation and development within the face-sheets. This model included an enhanced non-linear shear model and a mixed-matrix damage initiation and propagation law. The cohesive elements approach is also used to simulate the inter-laminar delamination. Furthermore, a specific continuum damage model is developed to simulate the behaviour of the ATH/Epoxy core. This model accounts for the damage initiation and propagation as well as the residual strength after final failure. The numerical results were compared with the test data and a good correlation was obtained. The numerical model was also used to assess the contribution of each component of the sandwich structure to its energy absorption capacity.

Compression test on ATH/Epoxy core

Flatwise compressive characteristic of ATH/Epoxy core with 50 wt% ATH was studied. Note that the ATH amount was selected on the basis of a preliminary experimental study (not reported herein), which was conducted earlier to identify the optimum ATH amount that can be used to minimize the heat generated during the epoxy curing reaction. The square cross-section specimens of 51 × 51 mm dimensions with thickness of 25.4 mm were prepared according to the ASTM D1621-10 standard procedure [10]. Testing was carried out on the MTS testing machine with displacement rate of 2.5 mm/min. The uniform distributed load was applied on specimens by two flat and parallel plates (Fig. 1).

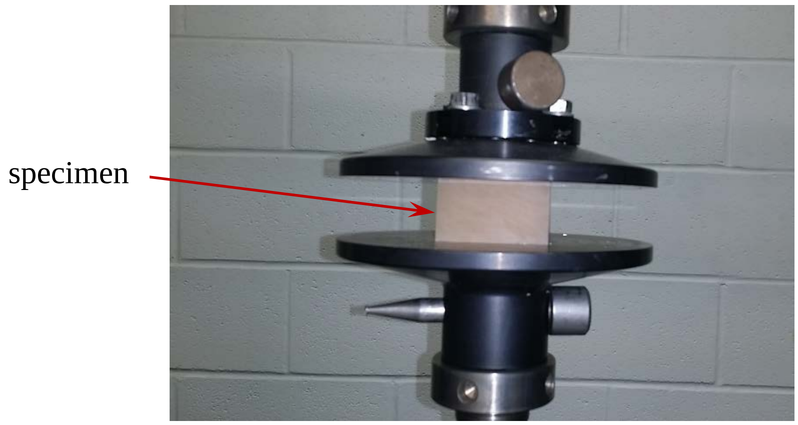

Fig. 1 Flatwise compression test setup

Fig. 2 depicts the load-displacement curves from compression testing experiments which served us to calculate the compressive Young's modulus and crush strength values.

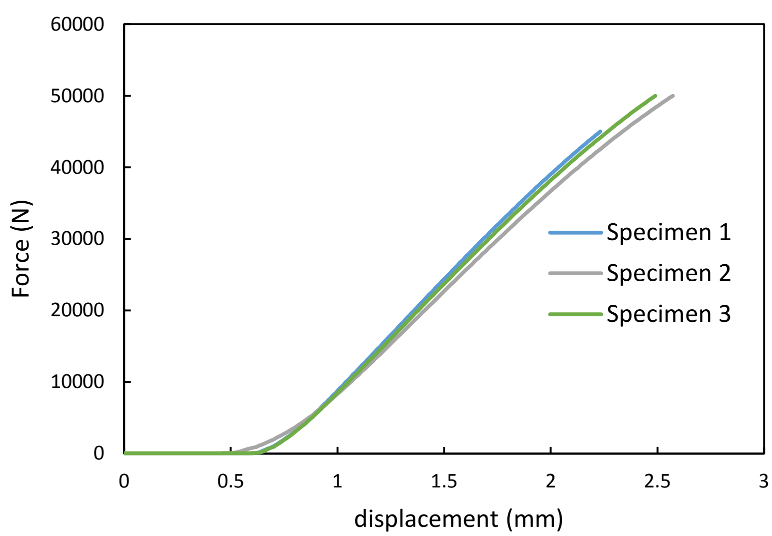

Fig. 2. Compressive force-displacement response of ATH/Epoxy

Face-sheets damage model

Material constitutive model and nonlinear shear response

For a better definition of the material constitutive model of composite laminates, both the non-linear behaviour due to the plastic deformation and the damage in the laminate must be considered [11]. These two phenomena can be simulated using plasticity and continuum damage theories, respectively. Thus, in the present work, elastic Hooke's law for linear orthotropic materials is adopted to contemplate the non-linear shear behavior.

The material constitutive model can be expressed as follows:

$$\begin{bmatrix}\sigma_{11}\\ \sigma_{22}\\ \sigma_{33}\end{bmatrix} = \frac{1}{\Omega}\begin{bmatrix} E_{11}(1-v_{23}v_{32}) & E_{22}(v_{12}-v_{32}v_{13}) & E_{33}(v_{13}-v_{12}v_{23}) \\ E_{11}(v_{21}-v_{31}v_{23}) & E_{22}(1-v_{13}v_{31}) & E_{33}(v_{23}-v_{21}v_{13}) \\ E_{11}(v_{31}-v_{21}v_{31}) & E_{22}(v_{32}-v_{12}v_{31}) & E_{33}(1-v_{12}v_{21}) \end{bmatrix}\begin{bmatrix}\varepsilon_{11}\\ \varepsilon_{22}\\ \varepsilon_{33}\end{bmatrix} \tag{1}$$

$$\Omega = 1 - v_{12}v_{21} - v_{23}v_{32} - v_{31}v_{13} - 2v_{21}v_{32}v_{13}$$

The nonlinear shear stress-strain part of the constitutive model is assigned as follows:

$$\tau_{ij} = G_{ij}\left(\gamma_{ij} - \gamma_{ij}^{in}\right)\left(1 - \alpha\gamma_{ij}\right) \ \ where \ \ ij = 1{,}2{,}3 \tag{2}$$

where γ_{ij} is total shear strain that can be decomposed into elastic γ_{ij}^{e} and inelastic components γ_{ij}^{in}:

$$\gamma_{ij} = \gamma_{ij}^{e} + \gamma_{ij}^{in} \tag{3}$$

Before damage initiation, inelastic component of the strain can be obtained by:

$$\gamma_{ij}^{in} = \gamma_{ij} - \frac{\tau_{ij}}{G_{ij}^{0}} - \frac{\tau_{ij}}{G_{ij}^{0}(1-\alpha\gamma_{ij})} \tag{4}$$

where G_{ij}^{0} is initial shear modulus, α is a material constant expressing the gradual shear modulus which can be found experimentally. To depict the nonlinear shear behaviour, a polynomial cubic stress-strain as follow was used:

$$\tau_{ij}(\gamma_{ij}) = c_1\gamma_{ij} + (\gamma_{ij})c_2\gamma_{ij}^{2} + c_3\gamma_{ij}^{3} \tag{5}$$

where c_1, c_2, and c_3 are the coefficients obtained by curve fitting to experimental shear stress-strain response.

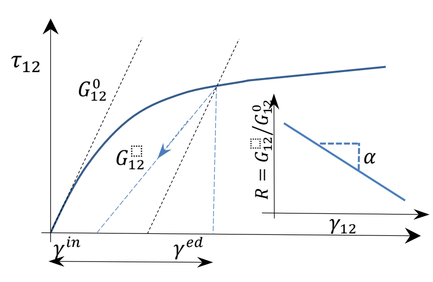

Fig. 3 Typical shear stress-strain response

Damage initiation and propagation in material constitutive was taken into account through the continuum damage mechanic model (CDM). Therefore, a physically-based CDM model was developed in the FE software. The continuous damage evaluation in each ply of laminate was described by a damage matrix D, which defined by three internal damage variables d_{ij} correspond to the different damage modes. Each of the damage variables reduces a component of the undamaged stress tensor σ to simulate the stiffness degradation.

$$\sigma^{d} = D\sigma \tag{6}$$

Intra-laminar damage model

Fibre failure modes

Two strain-based failure criteria, F_{11}^{T} and F_{11}^{C}, were used to detect fibre damage initiation under tensile and compressive loading, respectively:

$$\begin{gathered} F_{11}^{T} = \left(\frac{\varepsilon_{11}}{\varepsilon_{11}^{ot}}\right)^{2} - 1 \geq 0 \\ F_{11}^{C} = \left(\frac{\varepsilon_{11}}{\varepsilon_{11}^{oc}}\right)^{2} - 1 \geq 0 \end{gathered} \tag{7}$$

where ε_{11}^{ot} and ε_{11}^{oc} are the damage initiation strain in tension and compression, respectively.

Once the damage initiates, material starts to gradually lose its stiffness up to the final failure as sketched in Fig. 4. Here, the damage variables for tensile (d_{11}^{t}) and compressive (d_{11}^{c}) fibre failures are defined as follows:

$$\begin{gathered} d_{11}^{t} = \frac{\varepsilon_{11}^{ft}}{\varepsilon_{11}^{ft} - \varepsilon_{11}^{ot}}\left(1 - \frac{\varepsilon_{11}^{ot}}{\varepsilon_{11}}\right)^{2} \\ d_{11}^{c} = \frac{\varepsilon_{11}^{fc}}{\varepsilon_{11}^{fc} - \varepsilon_{11}^{oc}}\left(1 - \frac{\varepsilon_{11}^{oc}}{\varepsilon_{11}}\right)^{2} \end{gathered} \tag{8}$$

where ε_{11}^{ft} and ε_{11}^{fc} are the maximum strain at failure which are calculated as a function of the critical energy release rates (G_{11}^{t} and G_{11}^{c}), maximum longitudinal stresses (X^{t}, X^{c}) and the characteristic length, l^{*} as follows:

$$\varepsilon_{11}^{ft} = \frac{2G_{11}^{t}}{X^{t}\, l^{*}}\ ;\ \ \varepsilon_{11}^{fc} = \frac{2G_{11}^{c}}{X^{c}\, l^{*}} \tag{9}$$

One coupled tension-compression damage variable, d_{1f}, was used to simulate fibre degradation in the longitudinal direction:

$$d_{1f} = d_{11}^{c} + d_{11}^{t} - d_{11}^{t} d_{11}^{c} \tag{10}$$

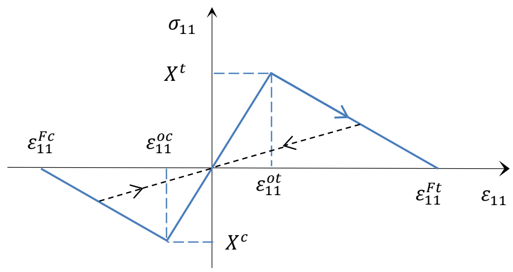

Fig. 4. Intra-laminar damage model behaviour for fiber failure

Matrix failure modes

Matrix damage initiation: Failure criterion proposed by Catalanotti et al. [12] was used to detect matrix cracking, F_{22}^{T}, and Puck failure criterion [13] was used to identify matrix crushing, F_{22}^{C}.

These criteria were defined as:

$$F_{22}^{T} = \left(\frac{\sigma_{\mathrm{nn}}}{S_{\mathrm{t}}^{is}}\right)^2 + \left(\frac{\tau_{\mathrm{nl}}}{S_{\mathrm{l}}^{is}}\right)^2 + \left(\frac{\tau_{\mathrm{nt}}}{S_{\mathrm{t}}^{is}}\right)^2 + \lambda\left(\frac{\sigma_{\mathrm{nn}}}{S_{\mathrm{t}}^{is}}\right)^2\left(\frac{\tau_{\mathrm{nl}}}{S_{\mathrm{l}}^{is}}\right)^2 + \kappa\left(\frac{\sigma_{\mathrm{nn}}}{S_{\mathrm{t}}^{is}}\right)^2 - 1 \geq 0$$

$$F_{22}^{C} = \left(\frac{\tau_{\mathrm{nl}}}{S_{\mathrm{l}}^{is} - \mu_{\mathrm{nt}}\sigma_{\mathrm{nn}}}\right)^2 + \left(\frac{\tau_{\mathrm{nt}}}{S_{\mathrm{t}}^{is} - \mu_{\mathrm{nl}}\sigma_{\mathrm{nn}}}\right)^2 - 1 \geq 0 \qquad (11)$$

where Y_t , S_{t}^{is}, and S_{l}^{is} are the matrix tensile strength and the *in situ* shear strength in transverse and longitudinal directions, respectively; κ and λ are defined as $\kappa = (S_l^2 - Y_t)/S_t\, Y_t$ and $\lambda = 2\mu_{nl}S_t/S_l - \kappa$; μ_{nt} and μ_{nl} are friction coefficients defined as $\mu_{nt} = -1/\tan(2\theta_f)$ and $\mu_{nl} = \mu_{nt}\, S_{12}/S_t$ where $S_t = Y_c/2\tan(\theta_f)$ and Y_c is the matrix compressive strength. The angle of fracture plane, θ_f, is approximately 53° for unidirectional laminate under pure compressive loading.

The two previous criteria depend on the stresses in the potential fracture plane (Fig. 5) which can be calculated using the standard transformation matrix $T(\theta)$:

$$\sigma_{nlt} = [T(\theta)]\sigma_{123}[T(\theta)]^T \qquad (12)$$

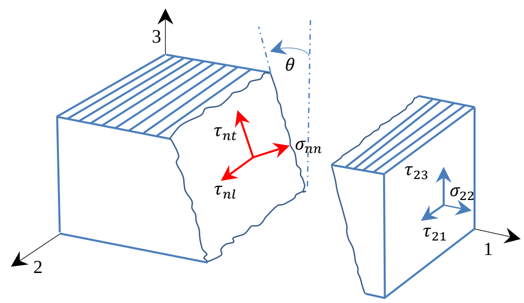

Fig. 5. Fracture plane in compression loading

<u>Matrix damage propagation:</u> when the matrix failure initiates under combined loading, the resulted stress, σ_r, and the corresponding strain, ε_r, on the potential fracture plan should be recorded as follows:

$$\begin{aligned} \sigma_r &= \sqrt{\langle\sigma_{nn}\rangle^2 + (\tau_{nt})^2 + (\tau_{nl})^2} \\ \varepsilon_r &= \sqrt{\langle\varepsilon_{nn}\rangle^2 + (\gamma_{nt})^2 + (\gamma_{nl})^2} \\ \varepsilon^0_{\mathrm{r,in}} &= \sqrt{(\gamma^{in}_{nt})^2 + (\gamma^{in}_{nl})^2} \end{aligned} \tag{13}$$

Here, $\varepsilon^0_{\mathrm{r,in}}$, is the inelastic component of the strain at the moment of failure initiation.

The matrix damage parameter, d_m, is defined as:

$$d_m = \frac{\varepsilon^f_{\mathrm{r}} - \varepsilon^0_{\mathrm{r,in}}}{\varepsilon^f_{\mathrm{r}} - \varepsilon^o_{\mathrm{r}}}\left(\frac{\varepsilon^0_{\mathrm{r}} - \varepsilon_r}{\varepsilon_r - \varepsilon^0_{\mathrm{r,in}}}\right) \tag{14}$$

The shear and tensile stresses on the fracture plane are reduced by the following relations and then they are transformed to the original plane.

$$\begin{aligned} \sigma_{nl} &= (1 - d_m)\sigma_{nl} \\ \sigma_{nt} &= (1 - d_m)\sigma_{nt} \\ \sigma_{nn} &= \sigma_{nn} - d_m\sigma_{nn} \end{aligned} \tag{15}$$

The fracture energy of the matrix, G_m, under combined stresses can be calculated as follows:

$$G_m = G_{IC}\left(\frac{\sigma_{nn}}{\sigma_r}\right)^2 + G_{IIc}\left(\frac{\tau_{nt}}{\sigma_r}\right)^2 + G_{IIC}\left(\frac{\tau_{nl}}{\sigma_r}\right)^2 \tag{16}$$

where G_{IC} and G_{IIC} are the critical strain energy release rates for modes I and II, respectively.

The final failure strain, ε^f_r, which is governed by the critical strain energy release rate, G_m, and characteristic length, l, is defined as follows:

$$\varepsilon_r^f = \frac{2G_m}{\sigma_r\, l} \tag{17}$$

Inter-laminar damage model

Cohesive elements —defined by a linear traction-separation model— are frequently used for simulating the delamination between two successive plies with different fiber orientations. This cohesive model is composed of an elastic behaviour until the damage initiation according to a stress-based quadratic interaction criterion, followed by decohesion of the two plies as a result of the damage propagation.

The quadratic stress-based criterion adopted herein to detect delamination initiation was defined as follows:

$$\left(\frac{\sigma_1}{T}\right)^2 + \left(\frac{\tau_2}{S}\right)^2 + \left(\frac{\tau_3}{S}\right)^2 = 1 \tag{18}$$

where σ_1, τ_2, τ_3 are the interface tangential and normal stresses and T, S are the maximum traction stresses in normal and tangential directions.

The delamination propagation was modeled using the Benzeggagh-Kenane rule [14] for mixed-mode loading:

$$\delta^F = \frac{1+\beta^2}{A_{TSLC}(T+\beta^2 S)}\left[G_{IC} + (G_{IIC} - G_{IC})\left(\frac{\beta^2 S}{T+\beta^2 S}\right)^{XMU}\right] \tag{19}$$

where β is the mixed mode ratio, XMU is exponent of the mixed mode criterion, A_{TSLC} is the area under the load-displacement curve, and G_{IC}, G_{IIC} are the inter-laminar fracture toughness in mode I, II.

ATH/Epoxy core damage model

In order to model the core damage behavior, some numerical approaches have been proposed in the open literature. Some authors [15, 16] applied a yield criterion that considers the transvers normal and shear stresses to predict the initiation of plasticity. Atkay et al. [8] proposed a removing failed element technique to simulate the damage propagation in honeycomb and foam cores. Nevertheless, this approach can not represent the residual strength of material after compressive failure. In this work, a damage model based on the continuum damage mechanic was proposed to simulate the damage initiation and propagation in ATH/Epoxy core. This model takes into account the residual strength after compression failure as sketched in Fig. 6.

The Besant's failure criterion [15] was adopted to detect the core failure initiation under combined shear and compression loads

$$\left(\frac{\sigma_{zz}}{\sigma_{cu}}\right)^2 + \left(\frac{\tau_{xz}}{\tau_{lu}}\right)^2 + \left(\frac{\tau_{yz}}{\tau_{tu}}\right)^2 \geq 1 \tag{20}$$

where σ_{cu}, τ_{lu}, and τ_{tu} are the corresponding yields stresses.

After damage initiation, the stresses (σ_{zz}, τ_{xz}, and τ_{yz}) are gradually reduced using a damage variable, d_c, defined as follows:

$$d_c = \frac{\varepsilon_c^f}{\varepsilon_c^f - \varepsilon_c^o}\left(1 - \frac{\varepsilon_c^o}{\varepsilon}\right)^2 \qquad (21)$$

where ε_c^o is the strain at the failure initiation and ε_c^f is the strain at the final failure.

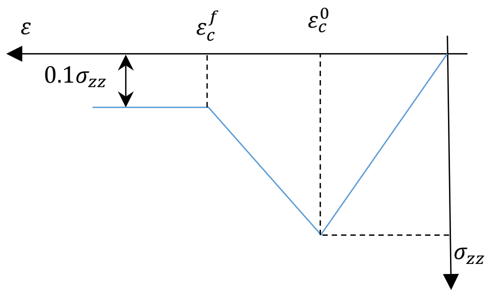

Fig. 6. Stress-strain response of the ATH/Epoxy core

Experimental details

In this investigation, non-crimp fabric (NCF) glass reinforced composite laminates are used as skins for sandwich panels. The composite skins were composed of six layers of E-glass/epoxy reinforcement. Each NCF lamina consists of three plies of [90°/0°/90°] tied together using polyester yarn. At first, the composite skins were manufactured using the vacuum infusion (VI) process. Meantime, sandwich core was prepared by mixing the resin epoxy with 50 wt% of ATH particles. The polymerization mixture was poured into a wood mould where the skins are earlier positioned at its both ends as sketched in Fig. 7. The nominal thickness of sandwich core is 34 mm. After the casting process was completed, the curing of the plastic core (ATH/Epoxy) was achieved at room temperature for 24h. Following the curing process, the sandwich panels were cut into specimens with 100 mm × 100 mm in dimension.

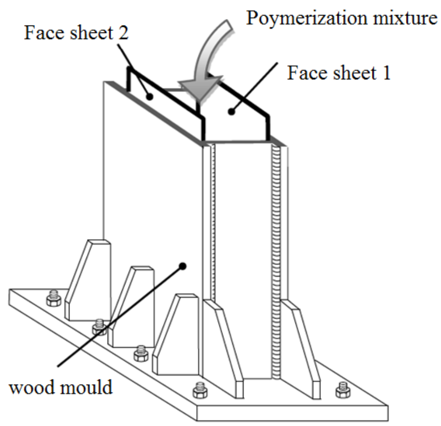

Fig. 7. Wood mould for fabrication of sandwich panel

Impact tests were performed using a drop weight machine following the guideline given in the ASTM standard D3763 [17]. The impactor had a mass of 22 kg and a diameter of 25.4 mm. During impact test, the specimen was constrained between two parallel rigid supports with a hole of 75 mm diameter in the center (see Fig. 8). A sufficient clamping pressure was applied to prevent slippage of the specimen during experiments.

Fig. 8 Specimen fixture apparatus

Finite element model

A 3D finite element model was implemented in LS-DYNA/Explicit code to predict the structural behavior of the whole sandwich panels as well as the damage characteristics for the core and face-sheets during impact loading. To decrease the computational time, only one quarter of the sandwich panel with symmetric boundary conditions was modelled as illustrated in Fig. 9.

Both the plastic core and face-sheets were modelled using eight-node solid elements with reduced integration and hourglass control. Zero-thickness cohesive elements were used to simulate delamination between adjacent plies with different fiber orientations. The impactor and support plate are defined to be rigid bodies. A surface-to-surface type contact element was defined between the upper face-sheet and the impactor surface.

Since no damage was observed in the bottom face-sheet following the experimental testing, the face-sheets damage model was only defined for the upper face-sheet. The ATH/Epoxy core behaviour was simulated through the core material model described in the previous section.

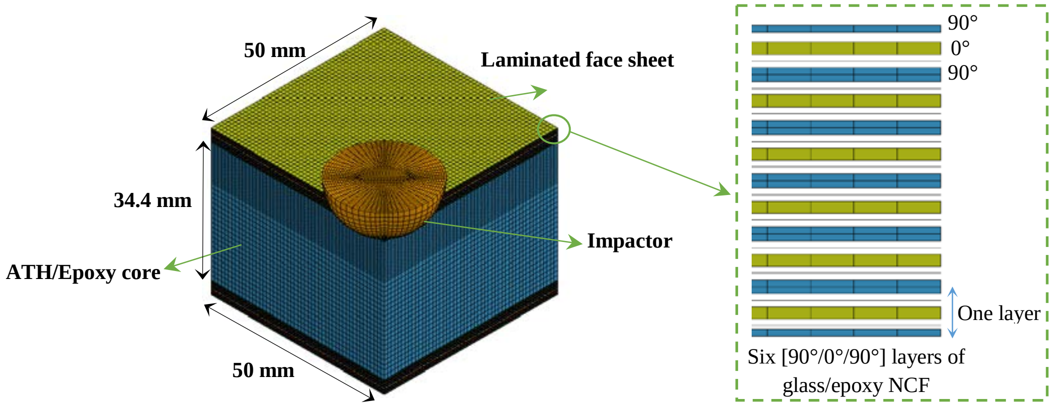

Fig. 9. Finite element model for impact simulations

Results and discussions

Impact response of ATH/Epoxy core

In order to validate the damage model proposed to simulate the AHT/Epoxy damage behavior, impact tests on the ATH/Epoxy specimens were performed for an impact energy of 21J. The choice of this energy level was made to avoid damaging of the used cell load since no data are available in the open literature regarding the impact resistance of the studied sandwich construction.

Figs. 10a and b present a comparison between numerical and experimental force-time curves and energy-time curves, respectively. In general, close correlation is achieved between the numerical prediction and the experimental data. The maximum recorded contact force is about 22.5 kN which can be considered as a high impact load.

Moreover, with regards to impact energy, the experimental results show that about 9.5J energy was absorbed through plastic deformations and matrix damage in the ATH/Epoxy core. Numerical model tends to underestimate the value of absorbed energy as is evident in Fig. 10b. The difference between numerical predictions and experimental data seems *a priori* due to an underestimation of the plastic deformation that the ATH/Epoxy material suffered during the test.

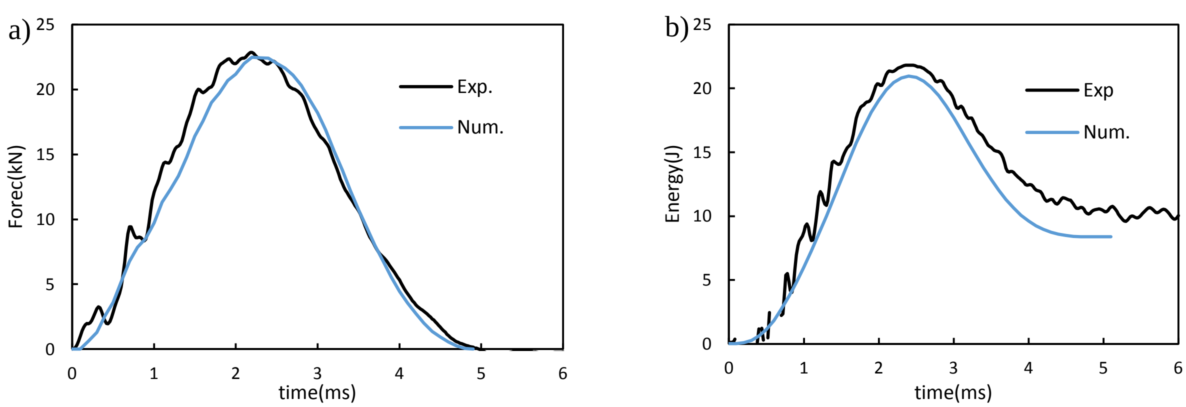

Fig. 9. Impact response of ATH/Epoxy core for an impact energy of 21J

A comparison between the experimental and predicted damage area at impact energy of 21J is presented in Fig. 11. The damage area reported herein represents the projected damage area towards the impacted surface. At first sight, it can be noticed that the numerical model is able to capture the shape (circular shape) and size of the damage area. This pointed out the appropriateness of the proposed core material model to simulate the damage pattern in the ATH/Epoxy plastic core.

From the numerical results, it can be noticed that the predicted damage depth is equal to almost one-half of the predicted damage diameter. Thus, it can be assumed that the experimental damage depth is about 4.5 mm. Microscopic observations will be needed to confirm this hypothesis.

On the other hand, the numerical results show that the compressive stresses in the ATH/Epoxy core are highly intense in the localized contact area. One can therefore draws the conclusion that the damage in ATH/Epoxy core resulted from high compressive stresses under the impactor. Moreover, numerical results show the presence of an irreversible deformation of the ATH/Epoxy core close to the impact zone. This residual deformation is manifested as a permanent indentation of 0.3 mm depth.

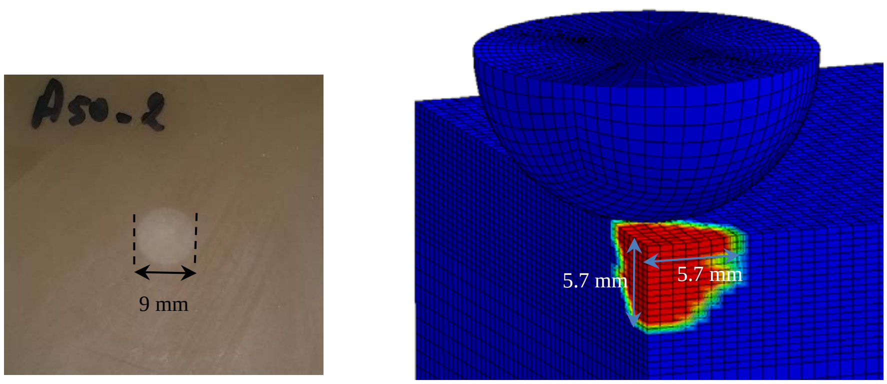

a) experimental damage zone b) numerical damage zone

Fig. 10. Damage zone in ATH/Epoxy specimen

Impact response of NCF laminated face sheet

In order to investigate the influence of sandwich core on the damage evolution in NCF glass/epoxy laminates face-sheets, the impact response of the face-sheets laminates was simulated herein under the same boundary conditions.

Fig. 12a and b illustrate the contact force and energy as a function of time for an impact energy of 21J. The predicted maximum contact force and absorbed energy are about 8.5 kN and 7.5J, respectively. The NCF composite laminates absorb energy through matrix damage and interface delamination mechanisms.

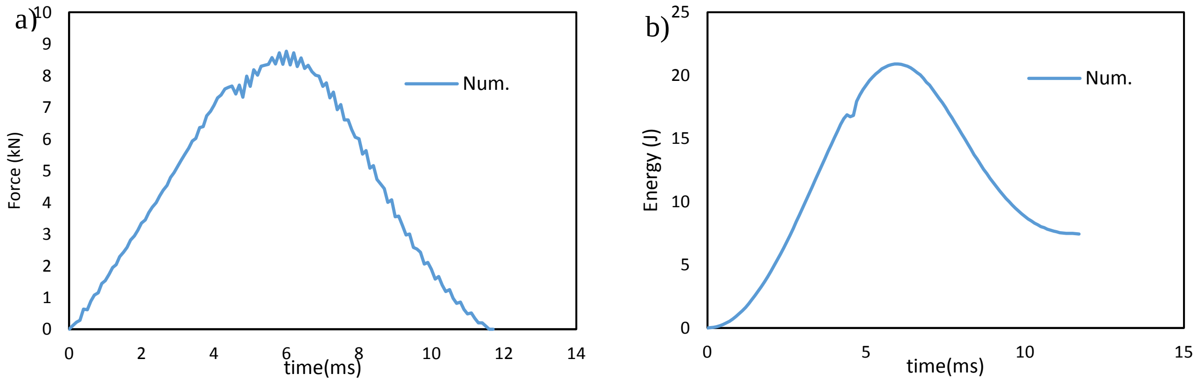

Fig. 11. Impact response of NCF laminated for an impact energy of 21J

Fig. 13 shows the predicted impact damage pattern in the NCF composite laminates. As can be seen in Fig. 13, the damage area is roughly circular with a diameter of 30 mm, which is relatively large damage area. The numerical results reveal that the matrix damage and delaminations are the main failure mechanisms in the NCF laminates for 21J impact energy. The high tensile stresses due to the large bending deformation are the main reason behind the matrix damage propagation.

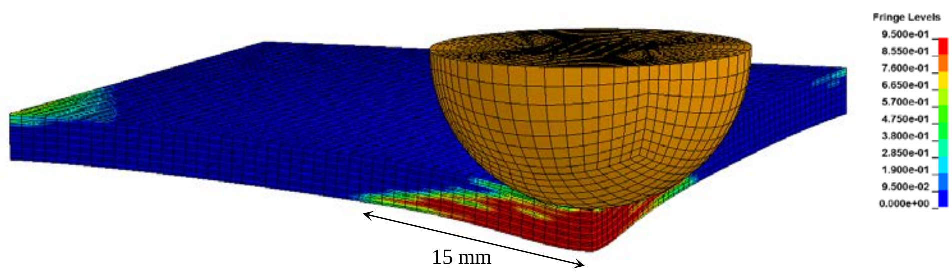

Fig. 12. Damage zone in NCF laminated

Impact response of the sandwich

Figs. 14a and b present the contact force-time and impact energy-time of the sandwich panel. As can be seen from Fig. 14a, there is a reasonable correlation between numerical predictions and experimental data. The maximum force is well predicted and its value is almost close to that achieved for the ATH/Epoxy specimen. The contact time, which is related to the material's resistance, is slightly shorter than that of ATH/Epoxy specimen. It seems that sandwich panel is a little stiffer than the ATH/Epoxy. From the experimental and numerical results, it was clear that the core material played an important role in the impact response of sandwich panel.

There is a smaller difference between the predicted and measured absorbed energy as shown in Fig. 14b. This difference is probably due to the plastic deformation in the core material. Beyond this, these results demonstrate the capacity of core material and sandwich panel to absorb energy. The sandwich panel absorbs more than half of impact energy. The absorbed energy is dissipated through face-sheets damage and core damage. The damage in the face-sheets was considerably reduced due to present of the ATH/Epoxy core (compare to NCF laminates only). Indeed, the nature of stress distribution is different from that of NCF laminates. The flexural deformation in the face-sheets decreased due to core stiffness, and hence, the amount of the bending cracks significantly decreased. In contrast, the shear cracks, which result from the high transverse shear stresses, are more pronounced in this case.

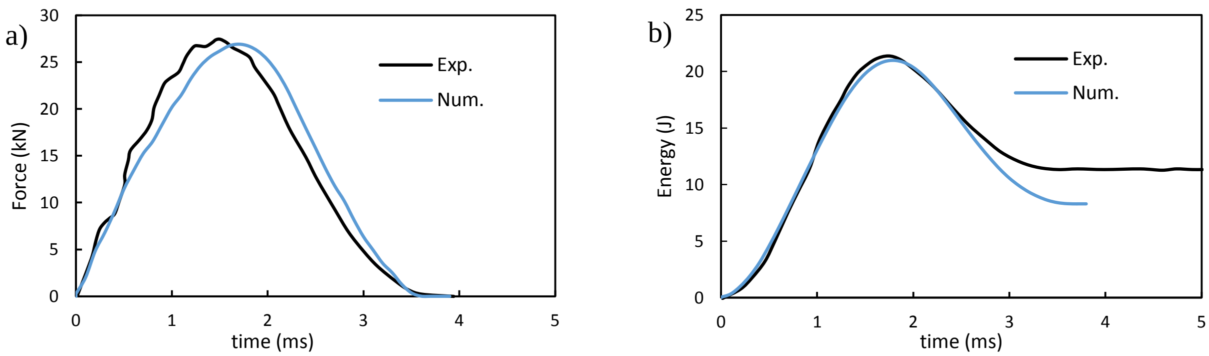

Fig. 13. Impact response of sandwich panel for an impact energy of 21J

The impact-damage areas in both the upper face-sheet and core are shown in Fig. 15. The damage pattern in the upper face-sheet is well predicted in terms of shape and size. Because of some experimental limitations, it was difficult to assess the impact-damage inside the core. However, since the damage model of the core was previously compared and validated with experimental data, the predicted damage in the core must be reasonably considered as reliable.

As expected, the size of damage area in the core is smaller than that of ATH/Epoxy specimen (without face-sheets) as shown in Fig. 15.

Moreover, the numerical results show a debonding failure at face-sheet/core interface close to the impact zone (Fig. 15a) where the shear stresses are the highest. It can therefore deduce that the sliding mode is the main cause of the interface debonding between the upper face-sheet and the core. The debonding zone is meanwhile relatively small. This could be due to the high elastic modulus of the ATH/Epoxy material. Indeed, the core's elastic modulus has a considerable effect on the interface debonding resistance [18].

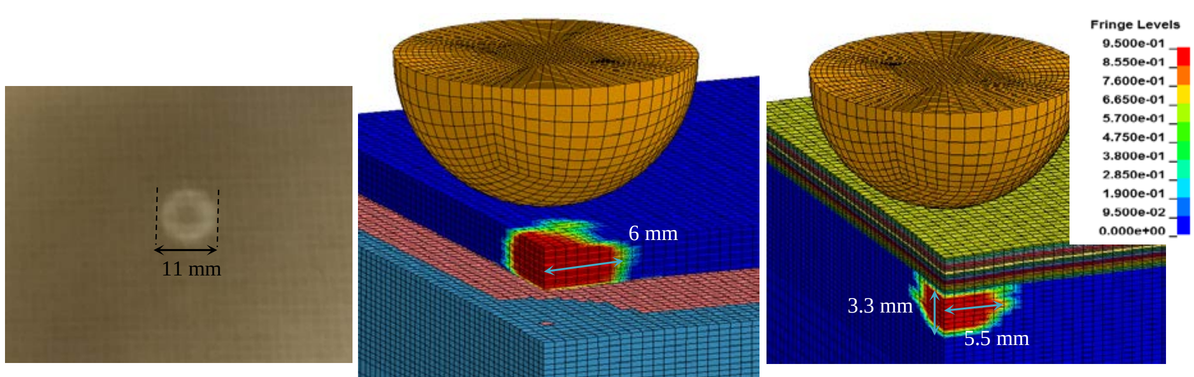

a) Experimental face sheet damage b) Face sheet damage c) core damage

Fig. 14. Damage zone in sandwich panel

In order to highlight the role of the plastic core on the energy dissipation process under impact loads, the energy dissipation in each component of the sandwich panel is tracked. Fig. 16 displays the energy dissipated in the core and the face-sheets along with the total energy dissipated in the sandwich panel for 21J impact energy. According to these energy curves, it was found that the energy dissipated in the ATH/Epoxy core is almost two times more than that dissipated in the face-sheets. Furthermore, more than 25% of the initial kinetic energy is absorbed in core crush (which was about 65% of the overall absorbed energy). However, less than 12% of the initial kinetic energy is absorbed in the upper face-sheet damage. These numerical findings are consistent with the previous results that reveal that the ATH/Epoxy has a good ability to locally deform and hence can absorbed a considerable amount of the energy dissipated in the whole structure.

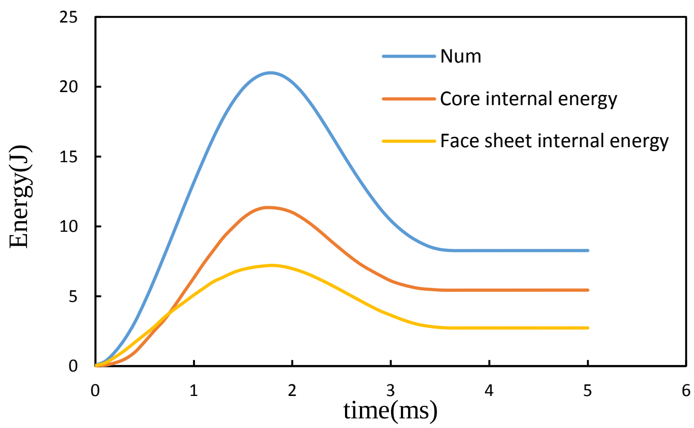

Fig. 15. Damage dissipation mechanism for an impact energy of 21J

Conclusions

A 3D progressive damage model was implemented into FEM software LS-DYNA/Explicit to predict the face-sheets and core damage in ATH/Epoxy core sandwich panels subjected to low-velocity impact loads. A continuum damage model was used to describe the behaviour and failure of the NCF glass/epoxy composite face-sheets, accounts for matrix damage, delamination, and fiber failure. Besides this, a damage model was developed to simulate the ATH/Epoxy behaviour which includes damage initiation and propagation and residual compressive strength. Experimental tests were conducted to validate the numerical model. In general, a reasonable correlation between the experimental data and the numerical simulations was achieved. The damage model used to simulate damage propagation in the face-sheets, has reflected accurately the experimental damage in the face-sheet. The numerical model of ATH/Epoxy predicted the damage and the absorbed energy in ATH/Epoxy specimens precisely.

Form experimental and numerical results, it can be drawn that ATH/Epoxy core sandwich panels are effective structure at withstanding low-velocity impact with relatively high impact energy. The ability of the ATH/Epoxy material to locally deform and absorb a large amount of impact energy makes them a suitable choice for the sandwich core when impact damage resistance is the main design issue.

The work presented in this paper is the first step in the development of a novel generation of hydraulic turbines components made from composite sandwich structures capable to better withstands impact loads.

References

[1] Chai, G. B., and Zhu, S., 2011, "A review of low-velocity impact on sandwich structures," Proceedings of the Institution of Mechanical Engineers, Part L: Journal of Materials Design and Applications, 225(4), pp. 207-230.

[2] Mines, R., Worrall, C., and Gibson, A., 1998, "Low velocity perforation behaviour of polymer composite sandwich panels," International Journal of Impact Engineering, 21(10), pp. 855-879.

[3] Crupi, V., Kara, E., Epasto, G., Guglielmino, E., and Aykul, H., 2015, "Prediction model for the impact response of glass fibre reinforced aluminium foam sandwiches," International Journal of Impact Engineering, 77, pp. 97-107.

[4] Evans, A. G., He, M., Deshpande, V. S., Hutchinson, J. W., Jacobsen, A. J., and Carter, W. B., 2010, "Concepts for enhanced energy absorption using hollow micro-lattices," International Journal of Impact Engineering, 37(9), pp. 947-959.

[5] Torre, L., and Kenny, J., 2000, "Impact testing and simulation of composite sandwich structures for civil transportation," Composite structures, 50(3), pp. 257-267.

[6] Zhou, J., Hassan, M. Z., Guan, Z., and Cantwell, W. J., 2012, "The low velocity impact response of foam-based sandwich panels," Composites science and Technology, 72(14), pp. 1781-1790.

[7] Foo, C., Chai, G., and Seah, L., 2008, "A model to predict low-velocity impact response and damage in sandwich composites," Composites science and Technology, 68(6), pp. 1348-1356.

[8] Aktay, L., Johnson, A. F., and Holzapfel, M., 2005, "Prediction of impact damage on sandwich composite panels," Computational Materials Science, 32(3), pp. 252-260.

[9] Feng, D., and Aymerich, F., 2013, "Damage prediction in composite sandwich panels subjected to low-velocity impact," Composites Part A: Applied Science and Manufacturing, 52, pp. 12-22.

[10] ASTM, 2010, "Standard Test Method for Compressive Properties of Rigid Plastics," ASTM International.

[11] Donadon, M., Iannucci, L., Falzon, B. G., Hodgkinson, J., and de Almeida, S. F., 2008, "A progressive failure model for composite laminates subjected to low velocity impact damage," Computers & Structures, 86(11), pp. 1232-1252.

[12] Catalanotti, G., Camanho, P., and Marques, A., 2013, "Three-dimensional failure criteria for fiber-reinforced laminates," Composite structures, 95, pp. 63-79.

[13] Puck, A., and Schürmann, H., 1998, "Failure analysis of FRP laminates by means of physically based phenomenological models," Composites science and Technology, 58(7), pp. 1045-1067.

[14] Benzeggagh, M., and Kenane, M., 1996, "Measurement of mixed-mode delamination fracture toughness of unidirectional glass/epoxy composites with mixed-mode bending apparatus," Composites science and Technology, 56(4), pp. 439-449.

[15] Besant, T., Davies, G., and Hitchings, D., 2001, "Finite element modelling of low velocity impact of composite sandwich panels," Composites Part A: Applied Science and Manufacturing, 32(9), pp. 1189-1196.
[16] Kärger, L., Baaran, J., and Teßmer, J., 2007, "Rapid simulation of impacts on composite sandwich panels inducing barely visible damage," Composite structures, 79(4), pp. 527-534.
[17] ASTM, 2006, "ASTM D3763–2006. Standard test method for high speed puncture properties of plastics using load and displacement sensor," USA Standards Association International, USA.
[18] Goswami, S., and Becker, W., 2001, "The effect of facesheet/core delamination in sandwich structures under transverse loading," Composite structures, 54(4), pp. 515-521.